TU Delft

Delft University of Technology

A transient, closed-loop network of wireless, body-integrated devices for autonomous electrotherapy

Choi, Yeon Sik; Jeong, Hyoyoung; Yin, Rose T.; Avila, Raudel; Pfenniger, Anna; Yoo, Jaeyoung; Lee, Jong Yoon; Tzavelis, Andreas; Rwei, Alina Y.; More Authors

DOI
10.1126/science.abm1703

Publication date
2022

Document Version
Final published version

Published in
Science

Citation (APA)
Choi, Y. S., Jeong, H., Yin, R. T., Avila, R., Pfenniger, A., Yoo, J., Lee, J. Y., Tzavelis, A., Rwei, A. Y., & More Authors (2022). A transient, closed-loop network of wireless, body-integrated devices for autonomous electrotherapy. *Science*, *376*(6596), 1006-1012. https://doi.org/10.1126/science.abm1703

Important note
To cite this publication, please use the final published version (if applicable).
Please check the document version above.

Copyright
Other than for strictly personal use, it is not permitted to download, forward or distribute the text or part of it, without the consent of the author(s) and/or copyright holder(s), unless the work is under an open content license such as Creative Commons.

Takedown policy
Please contact us and provide details if you believe this document breaches copyrights.
We will remove access to the work immediately and investigate your claim.

This work is downloaded from Delft University of Technology.
For technical reasons the number of authors shown on this cover page is limited to a maximum of 10.

Green Open Access added to TU Delft Institutional Repository

'You share, we take care!' - Taverne project

https://www.openaccess.nl/en/you-share-we-take-care

Otherwise as indicated in the copyright section: the publisher is the copyright holder of this work and the author uses the Dutch legislation to make this work public.

BIOMEDICINE

A transient, closed-loop network of wireless, body-integrated devices for autonomous electrotherapy

Yeon Sik Choi[1,2,3]†, Hyoyoung Jeong[1,2]†, Rose T. Yin[4]†, Raudel Avila[5], Anna Pfenniger[6], Jaeyoung Yoo[1,2], Jong Yoon Lee[1,2,7], Andreas Tzavelis[1,2,8,9], Young Joong Lee[1,2], Sheena W. Chen[10,11], Helen S. Knight[4], Seungyeob Kim[1,2,12], Hak-Young Ahn[1,2,3], Grace Wickerson[1,2,13], Abraham Vázquez-Guardado[1,2], Elizabeth Higbee-Dempsey[14], Bender A. Russo[4], Michael A. Napolitano[10,11], Timothy J. Holleran[10,11], Leen Abdul Razzak[1,2,8], Alana N. Miniovich[4], Geumbee Lee[1,2], Beth Geist[6], Brandon Kim[7], Shuling Han[15,16], Jaclyn A. Brennan[4], Kedar Aras[4], Sung Soo Kwak[1,2]‡, Joohee Kim[1,2], Emily Alexandria Waters[8,17], Xiangxing Yang[18], Amy Burrell[6], Keum San Chun[18], Claire Liu[1,2,8], Changsheng Wu[1,2], Alina Y. Rwei[19], Alisha N. Spann[17], Anthony Banks[1,2], David Johnson[6], Zheng Jenny Zhang[15,16], Chad R. Haney[8,17], Sung Hun Jin[1,2,12], Alan Varteres Sahakian[8,20], Yonggang Huang[1,3,5,21], Gregory D. Trachiotis[11], Bradley P. Knight[6], Rishi K. Arora[6]*, Igor R. Efimov[2,4]*§¶, John A. Rogers[1,2,5,8,13,22]*

Temporary postoperative cardiac pacing requires devices with percutaneous leads and external wired power and control systems. This hardware introduces risks for infection, limitations on patient mobility, and requirements for surgical extraction procedures. Bioresorbable pacemakers mitigate some of these disadvantages, but they demand pairing with external, wired systems and secondary mechanisms for control. We present a transient closed-loop system that combines a time-synchronized, wireless network of skin-integrated devices with an advanced bioresorbable pacemaker to control cardiac rhythms, track cardiopulmonary status, provide multihaptic feedback, and enable transient operation with minimal patient burden. The result provides a range of autonomous, rate-adaptive cardiac pacing capabilities, as demonstrated in rat, canine, and human heart studies. This work establishes an engineering framework for closed-loop temporary electrotherapy using wirelessly linked, body-integrated bioelectronic devices.

All living systems function through the interaction of complex networks of physiological feedback loops to maintain homeostasis. Engineering approaches to treat disorders, such as those based on cardiac pacemakers, exploit conceptually similar methods for closed-loop control to enable autonomous, adaptive regulation of one or more essential physiological parameters to target set points without human intervention (*1*–*3*). These and other existing platforms have key limitations that follow from their reliance on conventional electronic hardware, monitoring schemes, and interfaces to the body. First, such systems often require physical tethers and percutaneous access points that may lead to systemic infections (*4*–*7*). Second, connections to external modules for power supply, sensing, control, and other essential functions constrain patient mobility and impede clinical care. Third, removal or replacement of electronic components (e.g., leads or batteries) demands surgical procedures that impose additional risks and burdens on patients (*8*, *9*). These features can extend the duration of hospitalization, often in intensive care units. For example, short-term bradyarrhythmias that commonly occur in the 5 to 7 days after cardiac surgery must be treated with temporary percutaneous pacing systems, typically prolonging hospital stays with limited ability to initiate physical therapy (supplementary text 1). Recently reported wireless, bioresorbable electronic implants for temporary therapies address some of these challenges, but they still require external, wall-plugged equipment for monitoring, power, and control (*10*–*16*).

We introduce a transient, closed-loop system that incorporates a time-synchronized, wireless network with seven key components: (i) a temporary, bioresorbable, stretchable epicardial pacemaker; (ii) a bioresorbable steroid-eluting interface that minimizes local inflammation and fibrosis (*17*); (iii) a subcutaneous, bioresorbable power harvesting unit; (iv) a set of soft, skin-interfaced sensors that capture electrocardiograms (ECGs), heart rate (HR), respiratory information, physical activity, and cerebral hemodynamics for physiological monitoring of the patient; (v) a wireless radiofrequency (RF) module that transfers power to the harvesting unit; (vi) a soft, skin-interfaced haptic actuator that communicates via mechanical vibrations; and (vii) a handheld device with a software application for real-time visualization, storage, and analysis of data for automated adaptive control. These components integrate into a fully implantable, bioresorbable module [(i) to (iii)]; a set of skin-interfaced modules [(iv) to (vi)]; and an external control module (vii).

Figure 1A illustrates the use of this system for temporary cardiac pacing. The bioresorbable module wirelessly receives power for epicardial pacing. A network of skin-interfaced modules transmits diverse physiological data to the control module via Bluetooth low energy (BLE) protocols for real-time data visualization and algorithmic control. A haptic module provides tactile feedback to the patient. After a period of therapy, the bioresorbable module dissolves in the body, and the skin-interfaced modules are removed by peeling them off the skin. These "transient" characteristics of the system eliminate the need for surgical removal and allow ambulatory end of treatment. Figure 1B illustrates the closed-loop scheme that interconnects these modules into a wireless network (table S1). Soft, flexible designs (Fig. 1C) enable placement of the modules onto various target locations of the body.

Figure 1D shows that the constituent materials of the bioresorbable module completely disappear in simulated biofluid consisting of phosphate-buffered saline (PBS). Results of in vivo studies are provided in fig. S1. As shown in Fig. 2A, the bioresorbable module consists of an RF power harvester, which includes an inductive receiver (Rx) coil [molybdenum (Mo)] and a PIN diode [silicon nanomembrane

Downloaded from https://www.science.org at Delft University on June 14, 2022

[1]Center for Bio-Integrated Electronics, Northwestern University, Evanston, IL 60208, USA. [2]Querrey Simpson Institute for Bioelectronics, Northwestern University, Evanston, IL 60208, USA. [3]Precision Biology Research Center, Sungkyunkwan University, Suwon 16419, Republic of Korea. [4]Department of Biomedical Engineering, The George Washington University, Washington, DC 20052, USA. [5]Department of Mechanical Engineering, Northwestern University, Evanston, IL 60208, USA. [6]Feinberg School of Medicine, Cardiology, Northwestern University, Chicago, IL 60611, USA. [7]Sibel Health, Niles, IL 60714, USA. [8]Department of Biomedical Engineering, Northwestern University, Evanston, IL 60208, USA. [9]Medical Scientist Training Program, Feinberg School of Medicine, Northwestern University, Chicago, IL 60611, USA. [10]Department of General Surgery, The George Washington University, Washington, DC 20052, USA. [11]Department of Cardiothoracic Surgery, Veteran Affairs Medical Center, Washington, DC 20422, USA. [12]Department of Electronic Engineering, Incheon National University, 119 Academy-ro, Yeonsu-gu, Incheon 406-772, Republic of Korea. [13]Department of Materials Science and Engineering, Northwestern University, Evanston, IL 60208, USA. [14]Developmental Therapeutics Core, Northwestern University, Evanston, IL 60208, USA. [15]Comprehensive Transplant Center, Feinberg School of Medicine, Northwestern University, Chicago, IL 60611, USA. [16]Department of Surgery, Feinberg School of Medicine, Northwestern University, Chicago, IL 60611, USA. [17]Center for Advanced Molecular Imaging, Northwestern University, Evanston, IL 60208, USA. [18]Department of Electrical and Computer Engineering, University of Texas at Austin, Austin, TX 78712, USA. [19]Department of Chemical Engineering, Delft University of Technology, Van der Maasweg 9, 2629 HZ Delft, Netherlands. [20]Department of Electrical and Computer Engineering, Northwestern University, Evanston, IL 60208, USA. [21]Department of Civil and Environmental Engineering, Northwestern University, Evanston, IL 60208, USA. [22]Department of Neurological Surgery, Feinberg School of Medicine, Northwestern University, Chicago, IL 60611, USA.
***Corresponding author. Email: r-arora@northwestern.edu (R.K.A.); efimov@gwu.edu (I.R.E.); jrogers@northwestern.edu (J.A.R.)**
†These authors contributed equally to this work.
‡Present address: Center for Bionics of Biomedical Research Institute, Korea Institute of Science and Technology, Seoul 02792, Korea.
§Present address: Department of Biomedical Engineering, Northwestern University, Evanston, IL 60208, USA.
¶Present address: Department of Medicine, Division of Cardiology, Feinberg School of Medicine, Northwestern University, Chicago, IL 60611, USA.

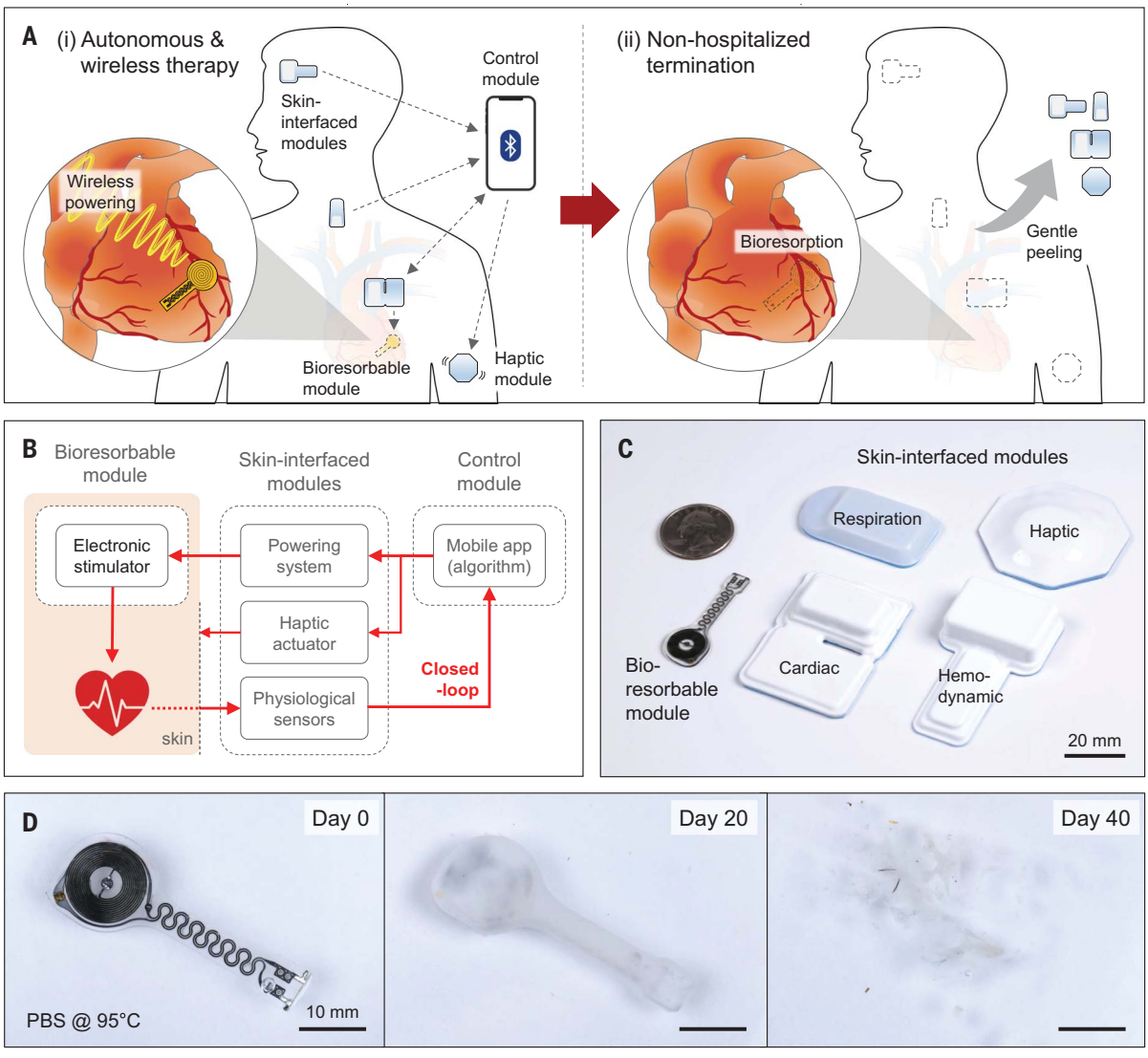

Fig. 1. Transient closed-loop system for temporary cardiac pacing. (**A**) Schematic illustration of a system for (i) autonomous and wireless pacing therapy and (ii) nonhospitalized termination. (**B**) Operational diagram of the closed-loop system for continuous monitoring, autonomous treatment, and haptic feedback. (**C**) Photographs showing the sizes of the various modules, relative to a US quarter. (**D**) Photographs of a bioresorbable module at different time points during immersion in a simulated biofluid (in PBS at 95°C).

(Si NM)], a pair of stretchable interconnects (Mo), and stimulation electrodes that integrate a steroid-eluting patch at the myocardial interface. The thin, lightweight, and stretchable design minimizes the possibility for irritation or damage at the tissue interface, with geometries that can be tailored to the anatomy of the patient (fig. S2). Figure 2B shows scattering parameters (S_{11}) of power harvesters with three different sizes of Rx coils (supplementary text 2). Continuous alternating current applied to a transmission (Tx) coil wirelessly delivers power to the Rx coil via magnetic induction and induces an approximately direct current monophasic output defined by the diode rectifier (Fig. 2C). The magnetic resonance imaging (MRI) compatibility of this wireless system is discussed in supplementary text 3. Top and bottom encapsulating layers of a bioresorbable dynamic covalent polyurethane (b-DCPU) and stretchable electrodes (*11*) ensure reliable pacing against the mechanically dynamic surface of the heart (*18*). Figure 2D shows negligible differences in output voltage during mechanical deformation, consistent with modeling results (fig. S7). Because the wireless energy transfer is inversely proportional to the coil-to-coil distance (fig. S8), the power harvester resides subcutaneously to maximize the efficiency. Poly(lactic-co-glycolic acid) (PLGA)–based steroid-eluting patches release dexamethasone acetate (DMA) over the course of several months to minimize local inflammation and fibrosis during cardiac pacing (Fig. 2E and fig. S9). The slow rate of dissolution of the bioresorbable conductor (Mo) enables >1 month of functional lifetime under simulated physiological conditions (Fig. 2F and supplementary text 4).

A network of skin-interfaced modules placed on various locations of the body acquires diverse data relevant to patient status. These collective data streams form the basis for closed-loop control. As the essential component, the cardiac module mounts on the chest to collect physiological information and to provide RF power to the bioresorbable module. Its materials and architectures (Fig. 2G and fig. S12) follow design principles of soft electronics to ensure robust, irritation-free coupling to the skin (fig. S13) at relevant locations (fig. S14) (*19*). The multihaptic module on the mid-medial forearm provides information on patient status and device operation through up to 625 patterns

Downloaded from https://www.science.org at Delft University on June 14, 2022

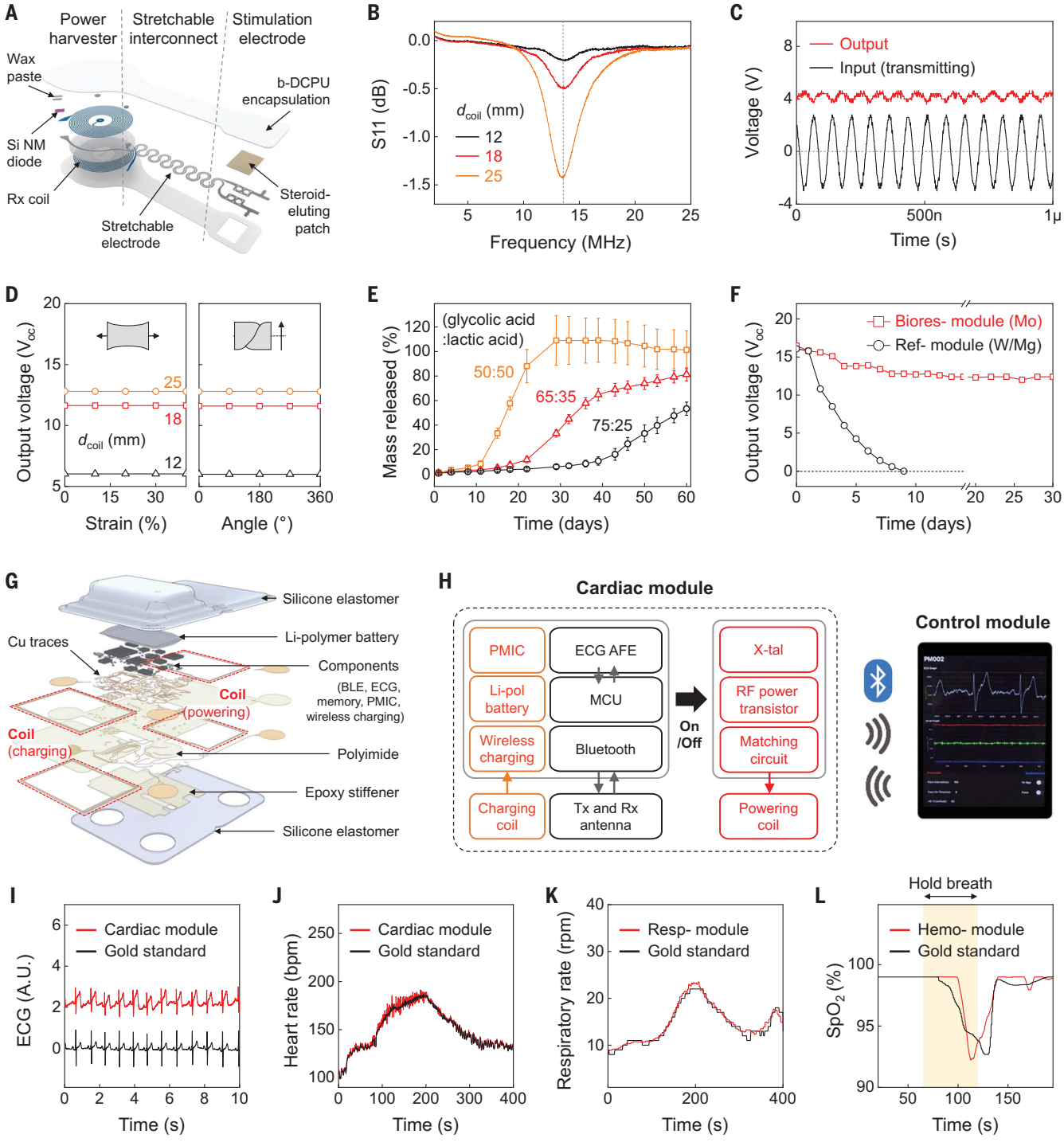

Fig. 2. Materials, design features. (**A**) Schematic illustration of a bioresorbable module. (**B**) S_{11} values of the Rx coils with different diameters (d_{coil}). (**C**) Example output waveform (red; d_{coil} = 12 mm) wirelessly generated by an alternating current (black; ~6 V_{pp}; 13.56 MHz) applied to the Tx coil. (**D**) Output open circuit voltage (V_{OC}) of devices as a function of tensile strain (left) and twist angle (right) at a fixed transmitting voltage (8 V_{pp}) and frequency (13.56 MHz). (**E**) Drug-release behaviors of steroid-eluting patches with three different ratios of base polymer. Error bars represent standard deviation. (**F**) Measurements of V_{OC} of the bioresorbable module (red squares; 10-μm-thick Mo) and a reference module (black circles; 700-nm-thick W coated 50-μm-thick Mg) immersed in PBS (37°C). (**G**) Schematic illustration of a skin-interfaced cardiac module. PMIC, power management integrated circuit. (**H**) System block diagram of the cardiac module. (**I** to **L**) Comparisons of ECG, HR, respiratory rate, and SpO_2 levels determined by the skin-interfaced modules [red; cardiac module in (I) and (J); respiratory module in (K); hemodynamic module in (L)] and a reference device (black). In (L), data were collected from a healthy subject who held their breath for 60 s (yellow background). A.U., arbitrary units; rpm, respirations per minute.

Downloaded from https://www.science.org at Delft University on June 14, 2022

of vibrotactile input (*20*). The respiratory module mounts at the suprasternal notch to capture physical activity, body temperature, and respiratory behavior in a dual-sensing design for accurate operation (*21*). The hemodynamic module on the forehead measures peripheral blood oxygen saturation (SpO_2) (*22*).

Figure 2H shows a block diagram of the skin-interfaced cardiac module. An ECG analog front end (AFE) and a microcontroller unit (MCU) process measured data in real time to calculate the HR (fig. S15). A BLE-enabled user interface serves as a control unit that stores and displays ECG tracings and three-axis acceleration data associated with cardiac and

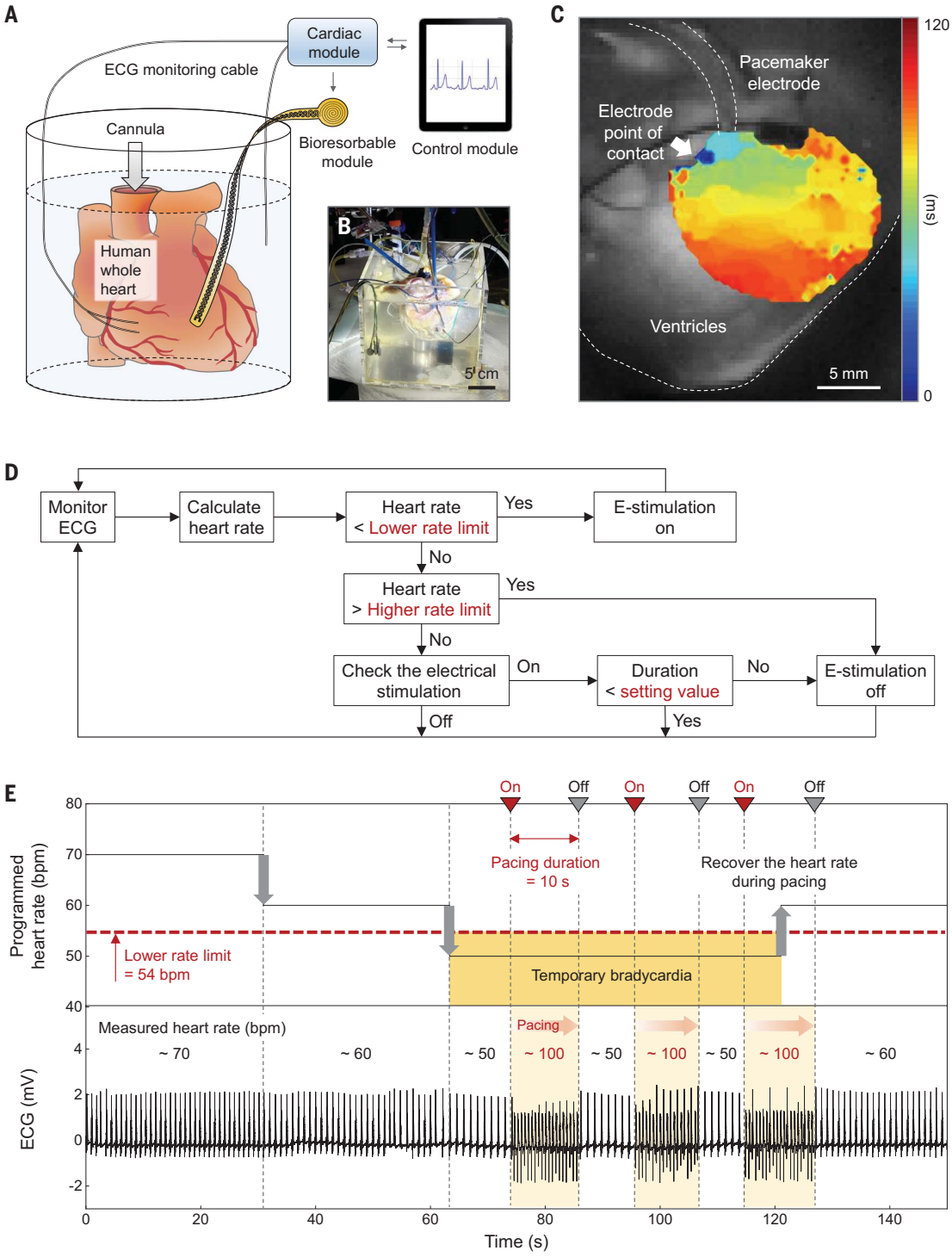

Fig. 3. Treatment of temporary bradycardia. (**A** and **B**) Schematic illustration (A) and photograph (B) of a Langendorff-perfused human whole-heart model with a transient closed-loop system (d_{coil} = 25 mm). (**C**) Action potential maps obtained by optical mapping of the human epicardium. (**D**) Flow chart of closed-loop hysteresis pacing to activate the pacemaker upon automatic detection of temporary bradycardia (supplementary text 8). (**E**) Programmed HR (top) and measured ECG (bottom) of a human whole heart. Set parameters are as follows: The lower rate limit is 54 bpm, pacing duration is 10 s, and pacing rate is 100 bpm.

Downloaded from https://www.science.org at Delft University on June 14, 2022

respiratory activity (fig. S16). Figure 2, I to K, shows that the skin-interfaced modules and data analytics approaches accurately determine HR and respiratory rate (fig. S17). The hemodynamic module yields SpO_2 data comparable to that recorded by a medical-grade finger probe (Fig. 2L). These systems use current best practices to protect health data, from the sensor, BLE link, phone, cloud, and beyond. To ensure secure medical data storage and processing, the interface application is compatible with hypertext transfer

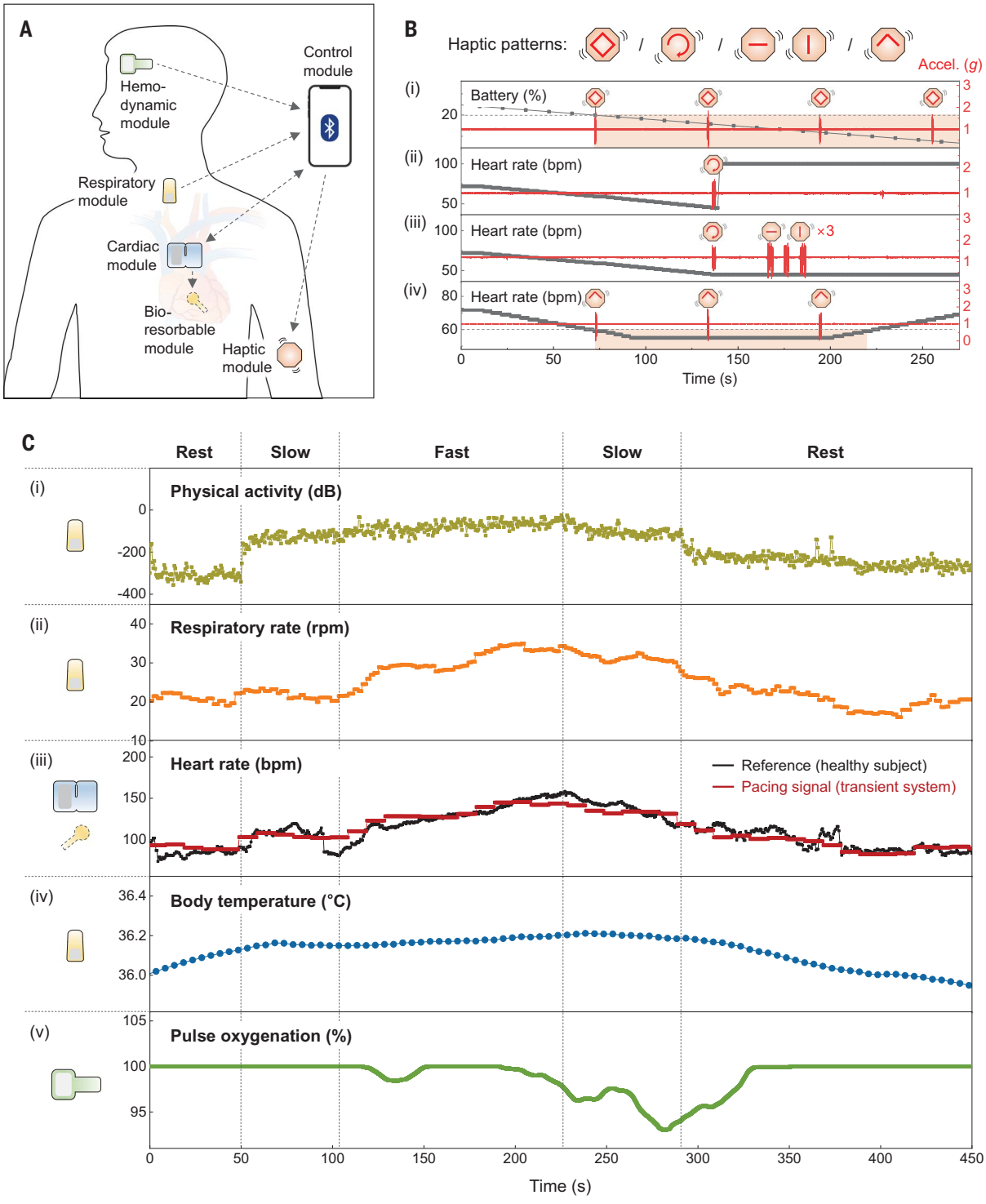

Fig. 4. Patient feedback and adaptive pacing functions. (**A**) Schematic illustration of a transient closed-loop system with the full collection of skin-interfaced modules. (**B**) Demonstration of the patient-awareness function using a multihaptic module. Accelerometer data (*g*) corresponds to vibrations (*z* axis) of the haptic actuators. (**C**) Results of clinical tests with a healthy human subject: (i) calculated physical activity and (ii) respiratory rate using data from the respiratory module, (iii) comparison of the HR (black) of a healthy human subject monitored by the cardiac module and rate-adaptive pacing signals (red) processed from the algorithm, (iv) calibrated and measured changes in core body temperatures using data from the respiratory module, and (v) representative SpO_2 measurements from the hemodynamic module.

Downloaded from https://www.science.org at Delft University on June 14, 2022

protocol secure (HTTPS) transport layer security (TLS 1.2) and with algorithms for encryption and decryption (fig. S18). In-sensor encryption [advanced encryption standard–128 (AES-128)] and Health Insurance Portability and Accountability Act (HIPAA)–compliant cloud data storage further protect patient data.

One of the key features of this transient closed-loop system (*10*–*15*) is that the skin-interfaced cardiac module eliminates requirements for wall-plugged external hardware for power transfer and control of the implanted pacemaker (fig. S19). In vivo studies with a canine whole-heart model demonstrate its capabilities (fig. S20). When the wireless cardiac module generates pulsed alternating currents [6 peak-to-peak voltage (V_{pp})], the bioresorbable module rectifies the received waveform and delivers it to the myocardium-interface as a cathodic monophasic pulse (~4 mW) (supplementary text 5). Investigations using rodent models demonstrate continuous, long-term pacing and biocompatibility (supplementary text 6 and 7).

An additional capability of this system is in autonomous treatment based on algorithmic identification of ECG signatures of abnormal cardiac activity. For example, hysteresis pacing delivers programmed electrical stimuli if the intrinsic rate falls below a certain threshold (*23*). Ex vivo human whole-heart studies demonstrate this type of treatment for temporary bradycardia (Fig. 3). Anisotropic activation of the membrane potential confirms that the bioresorbable module is the driving source of cardiac activation (Fig. 3C).

A flow chart of the feedback control system (Fig. 3D) implemented in the mobile application describes the hysteresis pacing scheme by which the system recognizes bradycardia and activates pacing during the programmed period of treatment. A separate pacing electrode enables manual control of the HR to mimic bradycardia (fig. S40). Figure 3E shows that the transient closed-loop system detects bradycardia [in this case, the bradycardic threshold is set to 54 beats per minute (bpm)] and automatically initiates pacing (~100 bpm). After a predetermined pacing duration (10 s), the system automatically stops pacing and evaluates the underlying intrinsic ECG signals to determine the need for additional pacing treatment. When the heart recovers from temporary bradycardia, the system detects the normal HR (~60 bpm) and ceases to deliver on-demand pacing.

For advanced forms of operation, the control module wirelessly communicates with the full collection of skin-interfaced modules via BLE protocols in a manner that is expandable and customizable to accommodate wide-ranging types of devices with various actuation, feedback, and/or monitoring capabilities. The schematic illustrations in Fig. 4A and fig. S41 summarize the most sophisticated system configuration reported here. This network of modules also includes the option to deliver tactile inputs through different patterns of vibration (fig. S42 and movie S1) to inform the patient of (i) the remaining battery life, (ii) the proper operation of the cardiac module, (iii) instances of malfunction of the other modules, and (iv) symptoms of bradycardia (Fig. 4B). The haptic module can also be activated to facilitate positioning of the cardiac module during mounting, of particular importance in the course of device replacement for recharging (fig. S43).

Real-time monitoring of cardiopulmonary status and physical activity, along with other essential parameters enables elaborate schemes for rate-adaptive pacing (supplementary text 9). Exercise tests of healthy human subjects on stationary bicycles demonstrate this rate-adaptive function (fig. S44). Figure 4C shows a strong qualitative correspondence (i) between measured physical activity and exercise intensity (e.g., rest, slow, fast). The respiratory rate (ii) shows a time-delayed correlation to physical activity and has gradual changes at the transition of exercise intensities. The pacing signal (iii), calculated by (i) and (ii), shows good agreement with the HR of the healthy subject because the metabolic demand is consistent with the level of exercise intensity and respiration. Results from different human subjects (n = 8) confirm the reliability of this algorithm (fig. S46), and supplementary text 10 describes strategies for stable and reliable pacing. Other physiological parameters, such as body temperature (iv) and blood oxygen saturation level (v), provide additional information that is postoperatively useful for patients with limited cardiopulmonary reserve, slowly resolving pneumonia, or persistent supplemental oxygen requirements.

This transient, closed-loop system represents a distributed, wireless bioelectronics technology that provides autonomous electrotherapy over a time frame that matches postoperative needs. The operation involves coordinated operation of a network of skin-interfaced modules and a bioresorbable device in time-synchronized communication with a control platform. Data captured from various locations of the body yield detailed information on cardiopulmonary health and physical activity. The results define autonomous, rate-adaptive pacing parameters to match metabolic demand through wireless powering of the bioresorbable module; they also support feedback on device and physiological status through a multihaptic interface. The bioresorbable module for cardiac pacing undergoes complete dissolution by natural biological processes after a defined operating time frame. The skin-interfaced devices can be easily removed after patient recovery. This system provides a framework for closed-loop technologies to treat various diseases and temporary patient conditions in a way that can complement traditional biomedical devices and pharmacological approaches.

REFERENCES AND NOTES

1. K. Kaszala, K. A. Ellenbogen, *Circulation* **122**, 1328–1340 (2010).
2. R. Hovorka, *Diabet. Med.* **23**, 1–12 (2006).
3. A. D. Mickle *et al.*, *Nature* **565**, 361–365 (2019).
4. J. L. Austin, L. K. Preis, R. S. Crampton, G. A. Beller, R. P. Martin, *Am. J. Cardiol.* **49**, 301–306 (1982).
5. F. J. Lumia, J. C. Rios, *Chest* **64**, 604–608 (1973).
6. K. D. Donovan, K. Y. Lee, *Anaesth. Intensive Care* **13**, 63–70 (1985).
7. M. U. Braun *et al.*, *Pacing Clin. Electrophysiol.* **29**, 875–879 (2006).
8. K. A. McLeod, *Heart* **96**, 1502–1508 (2010).
9. E. Buch, N. G. Boyle, P. H. Belott, *Circulation* **123**, e378–e380 (2011).
10. Y. S. Choi *et al.*, *Nat. Biotechnol.* **39**, 1228–1238 (2021).
11. Y. S. Choi *et al.*, *Nat. Commun.* **11**, 5990 (2020).
12. J. Koo *et al.*, *Sci. Adv.* **6**, eabb1093 (2020).
13. Y. S. Choi, J. Koo, J. A. Rogers, *MRS Bull.* **45**, 103–112 (2020).
14. Y. S. Choi *et al.*, *Adv. Funct. Mater.* **30**, 2000941 (2020).
15. S. K. Kang *et al.*, *Nature* **530**, 71–76 (2016).
16. S.-W. Hwang *et al.*, *Science* **337**, 1640–1644 (2012).
17. H. G. Mond, J. R. Helland, K. Stokes, G. A. Bornzin, R. McVenes, *Pacing Clin. Electrophysiol.* **37**, 1232–1249 (2014).
18. E. K. S. Espe *et al.*, *J. Cardiovasc. Magn. Reson.* **15**, 82 (2013).
19. H. U. Chung *et al.*, *Nat. Med.* **26**, 418–429 (2020).
20. X. Yu *et al.*, *Nature* **575**, 473–479 (2019).
21. H. Jeong *et al.*, *Sci. Adv.* **7**, eabg3092 (2021).
22. A. Y. Rwei *et al.*, *Proc. Natl. Acad. Sci. U.S.A.* **117**, 31674–31684 (2020).
23. E. García-Izquierdo, S. Vilches, V. Castro, *Circulation* **135**, 711–713 (2017).

ACKNOWLEDGMENTS

We thank the Washington Regional Transplant Community, heart organ donors, and families of the donors. Our research would not be possible without their generous donations and support. We appreciate valuable advice from K. Bailey, a board-certified veterinary pathologist at Charles River. This work made use of the NUFAB facility of Northwestern University's NUANCE Center, which has received support from the SHyNE Resource (NSF ECCS-2025633), the International Institute for Nanotechnology (IIN), and Northwestern's MRSEC program (NSF DMR-1720139). Computerized tomography (CT) and MRI work were performed at the Center for Advanced Molecular Imaging (RRID:SCR_021192). **Funding:** This work was funded by National Institutes of Health grants 1K99HL155844-01A1 (Y.S.C.), R01-HL141470 (I.R.E. and J.A.R.), R01 HL140061 (R.K.A.), R01 HL125881 (R.K.A.), KL2TR001424 (A.P.), F30HL157066 (A.T.), and 5K99-HL148523-02 (K.A.); Ministry of Health & Welfare, Republic of Korea (Korea Health Industry Development Institute), grant HI19C1348 (Y.S.C. and H.-Y.A.); Leducq Foundation project RHYTHM (I.R.E. and J.A.R.); American Heart Association 18SFRN34110170 (R.K.A.); American Heart Association Predoctoral Fellowship 19PRE34380781 (R.T.Y.); National Science Foundation Graduate Research Fellowship 1842165 (R.A.); a Ford Foundation Predoctoral Fellowship (R.A.); Chan Zuckerberg Initiative DAF grant 2020-225578 (E.A.W.); and an advised fund of the Silicon Valley Community Foundation (E.A.W.). **Author contributions:** Conceptualization: Y.S.C., H.J., R.T.Y., R.K.A., I.R.E., J.A.R.; Investigation: Y.S.C., H.J., R.T.Y., A.P., Y.J.L., S.W.C., H.S.K., H.-Y.A., G.W., A.V.-G., E.H.-D., B.A.R., M.A.N., T.J.H., L.A.R., A.N.M., G.L., B.G., S.H., J.A.B., K.A., S.S.K., J.K., E.A.W., X.Y., A.Bu., C.L., C.W., A.N.S., D.J.; Software: R.A., J.Y., J.Y.L., A.T., S.K., B.K., K.S.C., A.Y.R.; Supervision: A.Ba., Z.J.Z., C.R.H., S.H.J., A.V.S., Y.H., G.D.T., B.P.K., R.K.A., I.R.E., J.A.R.; Writing – original draft: Y.S.C., H.J., R.T.Y., A.P., R.K.A., I.R.E., J.A.R.; Writing – review and editing: Y.S.C., H.J., R.T.Y., R.K.A., I.R.E., J.A.R. **Competing interests:** I.R.E. consults for Cardialen, Sana Biotechnology, Zoll,

Downloaded from https://www.science.org at Delft University on June 14, 2022

and AliveCor. **Data and materials availability:** All data are available in the main text or the supplementary materials.
License information: Copyright © 2022 the authors, some rights reserved; exclusive licensee American Association for the Advancement of Science. No claim to original US government works. https://www.science.org/about/science-licenses-journal-article-reuse

SUPPLEMENTARY MATERIALS

science.org/doi/10.1126/science.abm1703
Materials and Methods
Supplementary Text
Figs. S1 to S48
Table S1
References (*24*–*50*)
MDAR Reproducibility Checklist
Movie S1

View/request a protocol for this paper from *Bio-protocol*.

Submitted 30 August 2021; accepted 23 March 2022
10.1126/science.abm1703

Downloaded from https://www.science.org at Delft University on June 14, 2022

Science

A transient, closed-loop network of wireless, body-integrated devices for autonomous electrotherapy

Yeon Sik ChoiHyoyoung JeongRose T. YinRaudel AvilaAnna PfennigerJaeyoung YooJong Yoon LeeAndreas TzavelisYoung Joong LeeSheena W. ChenHelen S. KnightSeungyeob KimHak-Young AhnGrace WickersonAbraham Vázquez-GuardadoElizabeth Higbee-DempseyBender A. RussoMichael A. NapolitanoTimothy J. HolleranLeen Abdul RazzakAlana N. MiniovichGeumbee LeeBeth GeistBrandon KimShuling HanJaclyn A. BrennanKedar ArasSung Soo KwakJoohee KimEmily Alexandria WatersXiangxing YangAmy BurrellKeum San ChunClaire LiuChangsheng WuAlina Y. RweiAlisha N. SpannAnthony BanksDavid JohnsonZheng Jenny ZhangChad R. HaneySung Hun JinAlan Varteres SahakianYonggang HuangGregory D. TrachiotisBradley P. KnightRishi K. AroraIgor R. EfimovJohn A. Rogers

Science, 376 (6596), • DOI: 10.1126/science.abm1703

Better cardiac care

There is an unmet medical need for minimally invasive devices to aid patients with slow heart rates, particularly after cardiovascular surgery, because the lines required to connect internal electrodes with battery packs are a common cause of infection and extended hospitalization. Choi *et al*. developed a biodegradable, closed-loop, wireless micro-electro-mechanical system (Bio-MEMS) for heart rate monitoring and control (see the Perspective by Zimmermann). Because the devices allow for both monitoring and control of the heart rate, they can be reprogrammed on demand in response to physiological conditions using the onboard electronics. Furthermore, the batteries in the devices can be recharged wirelessly through the skin, fully eliminating the need for transcutaneous wires. —MSL

View the article online
https://www.science.org/doi/10.1126/science.abm1703
Permissions
https://www.science.org/help/reprints-and-permissions

Downloaded from https://www.science.org at Delft University on June 14, 2022

Use of this article is subject to the Terms of service

Science (ISSN) is published by the American Association for the Advancement of Science. 1200 New York Avenue NW, Washington, DC 20005. The title *Science* is a registered trademark of AAAS.
Copyright © 2022 The Authors, some rights reserved; exclusive licensee American Association for the Advancement of Science. No claim to original U.S. Government Works